Chapter 5

Fractal to Non-Fractal Morphological Transitions in Stochastic Growth Processes

José Roberto Nicolás-Carlock, Víctor Dossetti and
José Luis Carrillo-Estrada

Additional information is available at the end of the chapter

http://dx.doi.org/10.5772/67941

Abstract

From the formation of lightning-paths to vascular networks, diverse nontrivial self-organizing and self-assembling processes of pattern formation give rise to intricate structures everywhere and at all scales in nature, often referred to as fractals. One striking feature of these disordered growth processes is the morphological transitions that they undergo as a result of the interplay of the entropic and energetic aspects of their growth dynamics that ultimately manifest in their structural geometry. Nonetheless, despite the complexity of these structures, great insights can be obtained into the fundamental elements of their dynamics from the powerful concepts of fractal geometry. In this chapter, we show how numerical and theoretical fractal analyses provide a universal description to the well observed fractal to nonfractal morphological transitions in particle aggregation phenomena.

Keywords: aggregation, entropic/energetic forces, fractal growth, morphological transitions, universality

1. Introduction

In nature, fractal structures emerge in a wide variety of systexms as a local optimization of diverse growth processes restricted to the entropic and energetic inputs from the environment. Even more, the fractality of these systems determines many of their physical, chemical, and/or biological properties. Thus, to comprehend the mechanisms that originate and control the fractality is highly relevant in many areas of science and technology [1–3].

One of the most successful approaches to this problem employs stochastic growth processes of particle aggregation. In general, aggregation phenomena are out-of-equilibrium processes of fractal pattern formation that are ubiquitous in nature [4]. As such, since the introduction of the diffusion-limited aggregation (DLA) and ballistic aggregation (BA) models, a plethora of studies has been developed trying to understand the ultimate aspects of the aggregation dynamics that give rise to *self-similar* or fractal clusters, the relationship of this *fractality* with their physical and chemical properties, and the most effective methods and techniques to control the fractal growth.

In particular, one striking feature of these systems is the morphological transition that they undergo as a result of the interplay of the entropic and energetic aspects of their growth dynamics that ultimately manifest themselves in the geometry of their structure [5]. It is here, where despite of their complexity, great insight can be obtained into the fundamental elements of their dynamics from the powerful concepts of fractal geometry [6, 7].

One example of this is the well-known dielectric breakdown model (DBM) or generalized Laplacian growth model, which has importantly contributed to our understanding of far-from-equilibrium growth phenomena, to such extent that seemingly unrelated patterns found in nature, as river networks or bacterial colonies, are understood in terms of a single framework of complex growth [8, 9]. However, we are still in need for a complete scaling theory of growth for systems far-from-equilibrium, as well as a comprehensive description of the fractality of systems that exhibits fractal to nonfractal morphological transitions [10].

In this chapter, starting from the mean-field result for the fractal dimension of Laplacian growth, we present a theoretical framework for the study of these transitions. Using a statistical approach to fundamental particle-cluster aggregation dynamics, under which it is possible to create four nontrivial fractal to nonfractal transitions that will capture all the main features of fractal growth, we show that, regardless of their space symmetry-breaking mechanism, they are well described by a universal dimensionality function, including the Laplacian one.

In order to show this, we consider the following: first, we introduce a general dimensionality function that is able to describe the measured fractal dimensions and scaling of clusters generated form particle aggregation. Second, we apply this equation to a set of fractal to nonfractal morphological transitions, created by identifying the fundamental dynamics that drive the fractal growth in particle aggregation and by combining three fundamental *off-lattice* particle-cluster aggregation models, the DLA, BA, and a recently introduced infinite-range mean-field (MF) attractive model [11, 12] under two different schemes. Afterwards, the scaling of the clusters along the transitions is measured for different values of their control parameters using two standard methods: the two-point density correlation function and the radius of gyration. Finally, we show how all measurements for the scaling of the DLA-MF, and BA-MF transitions collapse to a single universal curve valid for any embedding Euclidean space, under the appropriate variable transformations of the general dimensionality function.

http://dx.doi.org/10.5772/67941

2. Fundamental models

In the Laplacian theory of growth, the growth probability at a given point in space, μ, is given by the spatial variation of a scalar field, ϕ, i.e., $\mu \propto |\nabla\phi|$. An example of such processes is the paradigmatic DLA model, where particles randomly aggregate one-by-one to a seed particle to form a cluster [8–10] (**Figure 1**). It has been found that the structure that emerges from this process exhibits self-similar properties described by a fractal dimension, D, only dependent on the Euclidean dimension, d, of its embedding space [13, 14] given by,

$$D(d) = \frac{d^2+1}{d+1}. \tag{1}$$

For $d = 2$, this expression predicts $D = 5/3 \approx 1.67$, different from the widely reported and numerically obtained value for off-lattice DLA, $D = 1.71$. Furthermore, it was found that D is highly dependent on the mean square displacement of the particles' trajectories, giving rise to a continuous screening-driven morphological transition that has been neatly described by extending the Laplacian theory to consider a general process where particles follow fractal

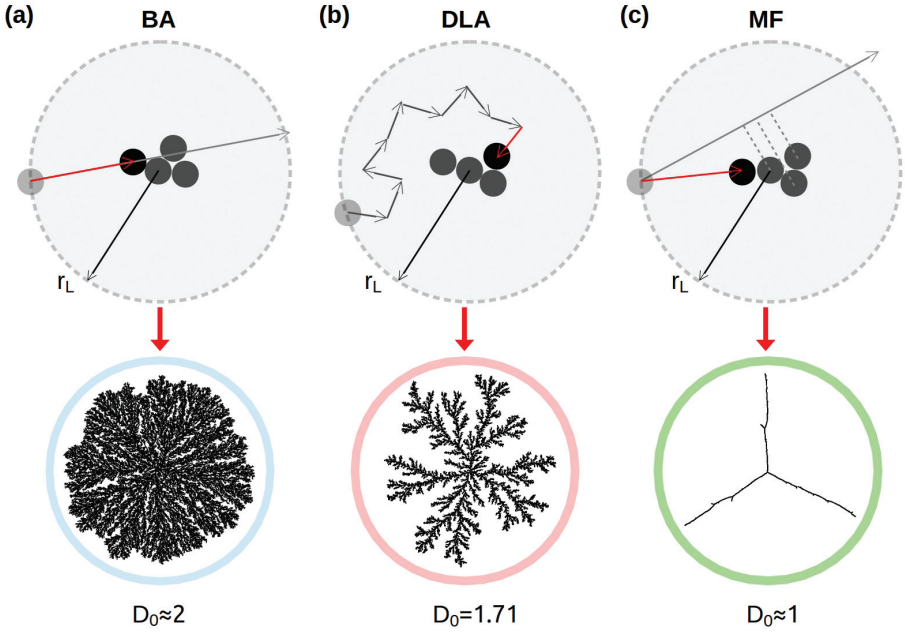

Figure 1. Schematic diagram of the fundamental aggregation models (top row) used in this work, where particles, that are launched one-by-one into the system from r_L with uniform probability in position and direction, (a) follow straight-line trajectories before aggregation in BA, (b) perform a random walk in DLA, and (c) get radially attached to the closest particle in the cluster as a result of an infinite-range radial interaction in MF. The morphology of MF emerges solely from its long-range interaction, as opposed to the stochastic BA and DLA. The corresponding characteristic cluster with its fractal dimension D_0 is shown in the bottom row.

trajectories [15]. It was found that D is related to the dimension of the walkers' trajectories, d_w, through the Honda-Toyoki-Matsushita (HTM) mean-field equation [16, 17]:

$$D(d, d_w) = \frac{d^2 + d_w - 1}{d + d_w - 1}. \tag{2}$$

Here, for $d_w = 1$ one gets $D = d$, as expected for ballistic-aggregation dynamics (see **Figure 1**), whereas for $d_w = 2$, the value $D = 5/3$ for DLA is recovered. This BA-DLA transition has been reproduced in diverse and equivalent aggregation schemes, e.g., of wandering particles under drift [18], or with variable random-walk step size [19], by imposing directional correlations [20, 21], and through probabilistically mixed aggregation dynamics [22].

However, one of the most challenging aspect of the theory comes when the growth is not purely limited by diffusion, e.g., when it takes place under the presence of long-range attractive interactions, where strong screening and anisotropic effects must be considered [1, 5, 7]. In this case, a clever generalization to the Laplacian growth process was proposed within the context of the DBM, assuming $\mu \propto |\nabla(\phi)|^{\eta}$, where η is a positive real number that keeps the information associated with all effects coming from screening and anisotropy [23, 24]. This process generates a characteristic fractal to nonfractal morphological transition from a compact structure with $D = d$ when $\eta = 0$, through DLA at $\eta = 1$, to a linear one with $D = 1$, as $\eta \to \infty$ [25, 26]. In this scenario, the generalized HTM equation [17, 27], given as,

$$D(d, d_w, \eta) = \frac{d^2 + \eta(d_w - 1)}{d + \eta(d_w - 1)}, \tag{3}$$

provides a good approximation to the dimensions of this transition but due to its mean-field limitations, it does not have a good correspondence with the numerical results [25, 26]. Nonetheless, as shown here, Eq. (3) is the starting point to clarify this aspect of the theory and, even, to establish a suitable and general framework to analyze more complex morphological transitions in stochastic growth processes.

This is done by considering that the fundamental dynamical elements of aggregation, which drive the fractal growth, are mainly two: a stochastic one, coming from the particles' trajectories randomness, and an energetic one, coming from attractive interactions. With regard to the latter, there are two physical mechanisms related to these interactions and two models that are able to reproduce their effects. First, the model we will refer to as λ-model [11], incorporates the screening effects associated to long-range attractive interactions (such as those coming from an attractive radial potential) by means of an effective interaction radius λ, as illustrated in **Figure 2a–c**. Second, the model referred here to as the p-model [12], incorporates anisotropy effects coming from surface-tension-like interactions by means of a Monte Carlo approach to aggregation using fundamental stochastic and energetic models as explained below and illustrated in **Figure 2d**. Therefore, by controlling the interplay of any of these two mechanisms with a pure stochastic model (in this case the DLA or BA models), one is able to generate fractal to nonfractal morphological transitions.

http://dx.doi.org/10.5772/67941

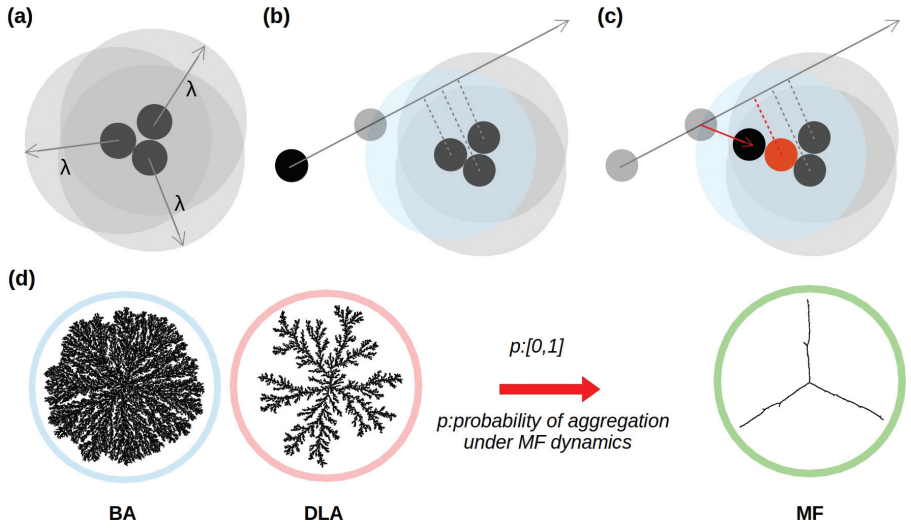

Figure 2. Schematic diagrams of the *energetic* aggregation schemes. For the λ-model: (a) every particle in the cluster is provided with an effective radius of aggregation λ. (b) A particle "collides" with the cluster when its trajectory intersects for the first time the interaction boundary of any aggregated particle. (c) The particle is aggregated to the closest particle along its direction of motion. This is determined by the position of the aggregated particles projected onto the direction of motion of the incoming particle. For the p-model: (d) a Monte Carlo approach to aggregation is established through the variable $p \in [0,1]$, that controls the probability of aggregation under MF dynamics.

3. Methods

In the following and as explained below, all data for D were measured over a large ensemble of clusters (with $N = 1.5 \times 10^5$ particles) for each value of the control parameters of the models proposed, by means of two standard methods: the two-point density correlation function, $C(r) \propto r^{-\alpha}$, and the radius of gyration, $R_g(N) \propto N^{\beta}$, where the scaling exponents are related to D as $D_\alpha = d - \alpha$, and $D_\beta = 1/\beta$.

3.1. Aggregation dynamics

In all of the numerical calculations, we choose as a unit of distance, the particles' diameter here is set to one. For generating aggregates based on BA or MF (**Figure 1a** and **1c**), a standard procedure was used in which particles are launched at random, with equal probability in position and direction of motion, from a circumference of radius $r_L = 2r_{\max} + \delta$, where $r_{\max}$ is the distance of the farthest particle in the cluster with respect to the seed particle at the origin. As well, we used $\delta = 1000$ particle diameters to avoid undesirable screening effects. On the other hand, for the MF model, particles always aggregate to the closest particle in the cluster. This is determined by projecting the position of the aggregated particles along the direction of motion of the incoming particle (see **Figure 1c**). Finally, in the

case of aggregates generated using DLA dynamics (**Figure 1b**), particles were launched from a circumference of radius $r_L = r_{max} + \delta$ with $\delta = 100$, while their mean free path was set to one particle diameter in the beginning. Further on, as typically done, their mean free path is modified as the particles wander beyond a distance larger than r_L or in-between branches. As well, a killing radius is set at $r_K = 2r_L$ in order to speed up the aggregation process. For the special case of the λ-model, for aggregates generated with DLA dynamics, particles were launched from a circle of radius $L = r_{max} + \lambda + \delta$, with $\delta = 100$.

Regarding the *p*-model, in order to mix different aggregation dynamics, a Monte Carlo scheme of aggregation is implemented using the BA, DLA, and MF models. The combination between pairs of models results in the DLA-MF and BA-MF transitions by varying the mixing parameter $p \in [0, 1]$. This parameter is associated with the probability or fraction of particles aggregated under MF dynamics, $p = N_{MF}/N$, where N is total number of particles in the cluster. Therefore, as p varies from $p = 0$ (pure stochastic dynamics given by the BA or DLA dynamics) to $p = 1$ (purely energetic dynamics given by the MF model), it generates two transitions discussed below. The evaluation of the aggregation scheme to be used is only updated once and the particle has been successfully aggregated to the cluster under a given dynamics.

3.2. Fractal and scaling analysis

In all measurements, we performed an ensemble average over 128 clusters containing 1.5×10^5 particles each. In first place, we measured the fractal dimension from the two-point density correlation function,

$$C(r) = \langle\langle \rho(\mathbf{r}_0)\rho(\mathbf{r}_0 + \mathbf{r})\rangle\rangle_{|\mathbf{r}|=r}, \tag{4}$$

where the double bracket indicates an average over all possible origins r_0 and all possible orientations. Here, it is assumed that $C(r) \approx r^{-\alpha}$, where the fractal dimension is given by $D_\alpha = d - \alpha$ with d being the dimension of the embedding space. In second place, we also measured the radius of gyration given by

$$R_g^2 = \sum_{i=1}^{N} (r_i - r_{CM})^2, \tag{5}$$

where N is the number of particles, r_i is the position of the ith-particle in the cluster and, r_{CM} is the position of the center of mass. Here, it is assumed that $R_g(N) \approx N^\beta$, where the fractal dimension is given by $D_\beta = 1/\beta$. In this way, the fractal dimensions D_α and D_β are, respectively obtained from linear-fits to the corresponding functions $C(r)$ and $R_g(N)$ in log-log plots at different scales.

In particular, for the *p*-model, linear-fits at different scales were performed in order to capture the main local fractal features. In addition, we averaged the results of 10 linear fits, distributed over a given interval, in order to improve the precision of the measurements. In both transitions, DLA-MF and BA-MF, $D_\alpha(p)$ was measured at short length-scales (regions α_I in **Figure 6**) over the interval $r_i \in [1, 2]$ with fitting-length equal to 10, and $r_f \in [11, 12]$ (in

http://dx.doi.org/10.5772/67941

particle diameters units). At long length-scales (α_{II}), over $r_i \in [10, 11]$ with fitting-length equal to 40, and $r_f \in [50, 51]$. For $D_\beta(p)$, measurements at medium scales (β_I) were performed over the interval $r_i \in [10^2, 10^3]$ with fitting-length equal to 10^4, and $r_f \in [1.01 \times 10^4, 1.1 \times 10^4]$ (in particle number). Finally, at large scales (β_{II}), over the interval $r_i \in [10^3, 10^4]$ with fitting-length equal to 0.9×10^5, and $r_f \in [9.1 \times 10^4, 10^5]$.

4. Fractality prescriptions

Despite the complexity leading to morphological transitions, simple models can be established to describe their fractality or scaling as a function of the control parameter, in our case, the branching parameter ε for the λ-model (see below) or the mixing parameter p for the p-model. To do so, let us start by showing that Eq. (3) can in fact be recovered as the first-order approximation in $f(\eta)/d$ of a general exponential form,

$$D(d) = 1 + (d-1)e^{-f(\eta)/d}, \tag{6}$$

with $f(\eta) = \Lambda\eta(d_w - 1)$. It easily follows that,

$$D(d) \approx 1 + \frac{d-1}{1+f(\eta)/d} = \frac{d^2 + f(\eta)}{d + f(\eta)}. \tag{7}$$

In this form, by setting $\Lambda = 1$, Eq. (3) can be fully recovered. Therefore, it is clear that $f(\eta)$ in Eq. (6) keeps all the information associated with the structural symmetry-breaking of the clusters in the DBM. Under this formalism, let us introduce $f(p)$ with control parameter p, which takes a similar role as $f(\eta)$, i.e., it is associated with the net effect of all screening/anisotropy-driven forces of a more complex growth process, not necessarily corresponding to the DBM description. For simplicity, we propose $f(p) = \Lambda p^\chi$, where $p \in [0, 1]$ is the parameter that controls the transition, and where Λ and χ are two positive real numbers associated with the strength of screening/anisotropy-driven forces, that are to be determined either theoretically or phenomenologically according to the studied transition. This allows us to define a general dimensionality function, $D(p)$, that describes the fractal dimension of a structure collapsing toward $D = 1$ under the effects of $f(p)$ as,

$$D(p) = 1 + (D_0 - 1)e^{-f(p)/D_0}, \tag{8}$$

where D_0, with $d \geq D_0 > 1$, is the fractal dimension of the clusters for $p = 0$. This equation predicts an inflection point at p_i, given by $(\Lambda/D_0)p_i^\chi = (\chi - 1)/\chi$, which defines the change in dynamical growth regimes. Additionally, the first-order approximation of Eq. (8), is,

$$D(p)^{(1)} = \frac{D_0^2 + f(p)}{D_0 + f(p)}, \tag{9}$$

with p_i given now by $(\Lambda/D_0)p_i^{\chi} = (\chi - 1)/(\chi + 1)$. Eqs. (8) and (9) describe a continuous morphological transition from $D = D_0$ for $f(p) = 0$ (disordered/fractal states) toward $D = 1$ as $f(p) \to \infty$ (ordered states), with a well-defined change in growth dynamics at p_i.

Furthermore, let us introduce the reduced parameter, $q = p/p_i$. Analytically, substituting $q \in [0,\infty)$, back into Eq. (8) leads to,

$$D(q) = 1 + (D_0 - 1)e^{-\Phi(q)}, \tag{10}$$

where

$$\Phi(q) = q^{\chi}(\chi - 1)/\chi, \tag{11}$$

is an effective parameter associated to a generalized screening/anisotropy-driven force. Its first-order approximation is then,

$$D(q)^{(1)} = \frac{D_0 + \Phi(q)}{1 + \Phi(q)}, \tag{12}$$

where the effective parameter is now given as,

$$\Phi(q) = q^{\chi}(\chi - 1)/(\chi + 1). \tag{13}$$

With this prescription, the dynamical change in growth regime is now located at $q_i = 1$ for all transitions. Here, we can also include the DBM transition as well, for which $\Phi(q) = q(d_w - 1)/d$.

5. Morphological transitions

5.1. The λ-model: screening-driven transition

In the first approach to morphological transitions, we will consider the case when long-range attractive interactions are introduced in the growth dynamics. In this case, the way to obtain self-similar clusters, that is, clusters with a single fractal dimension, is to maintain a proper balance between the energetic and entropic contributions to the growth process. This can be done by considering an aggregation radius, λ, associated with the range of the interaction for each particle in the growing cluster.

For example, for $\lambda = 1$, or *direct-contact* interaction, the usual DLA or BA models are recovered (see **Figure 3a** and **4a**, respectively). When $\lambda > 1$, the attractive interactions modify the local morphology of the aggregates, leading to a more stringy structure. Two well defined features emerge due to the interplay of the long-range interactions and the way particles approach the cluster (in relation with their trajectories): a *multiscaling* branching growth and a crossover in fractality, from $D \to 1$ (as $\lambda \to \infty$) to $D = D_0$ (when $N \to \infty$), as shown in **Figures 3** and **4**.

It can be appreciated that this growth presents three well-defined stages as illustrated in **Figures 3d** and **4d**. In the first one, the growth is limited by the interactions and is

http://dx.doi.org/10.5772/67941

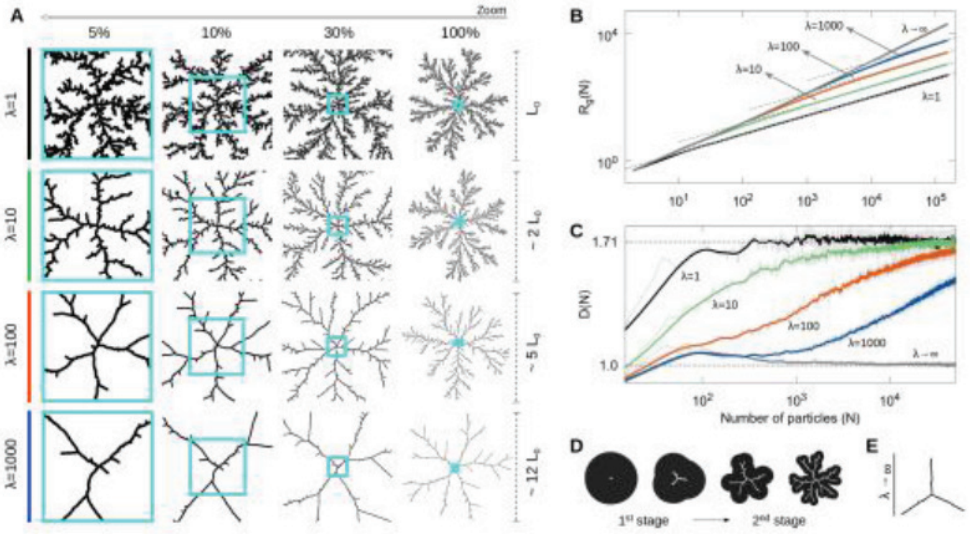

Figure 3. (a) Multiscaling aggregates based on DLA, containing $N = 150 \times 10^3$ particles each, for $\lambda = 1, 10, 100$ and 1000 units, visualized at 5, 10, 30 and 100% of their total size. The squares display the multiscaling evolution of the structure. (b) Radius of gyration, R_g, and (c) fractal dimension, D, versus the number of aggregated particles, N, in log-log and lin-log plots, respectively. Notice that, when $\lambda \to \infty$, the structure of the aggregates tends to MF ($D = 1$). (d) Evolution of the growing front for the first two stages of growth. (e) Typical structure of an MF aggregate.

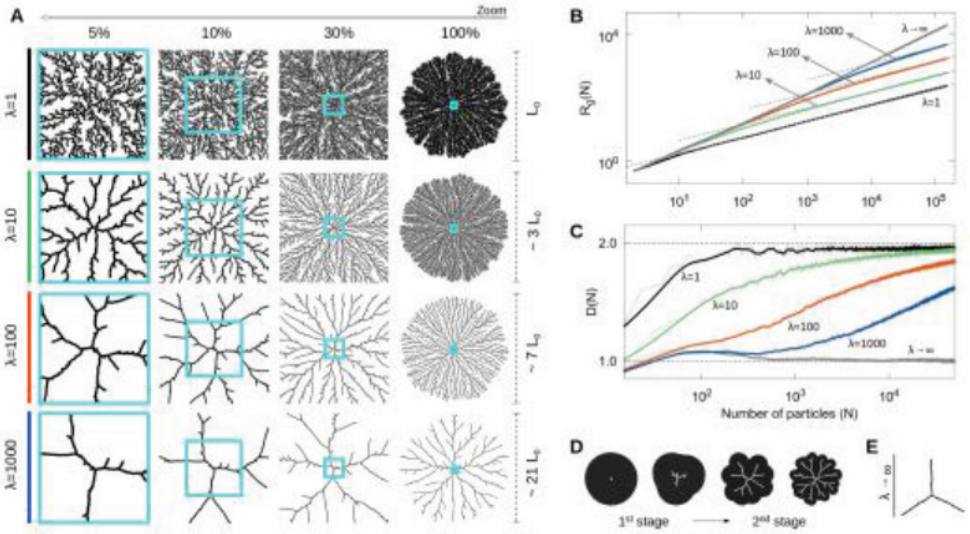

Figure 4. (a) Multiscaling aggregates based on BA, containing $N = 300 \times 10^3$ particles each, for $\lambda = 1, 10, 100$ and 1000 units, visualized at 5, 10, 30 and 100% of their total size. (b) Radius of gyration, R_g, and (c) fractal dimension, D, versus the number of aggregated particles, N, in log-log and lin-log plots, respectively. (d) Evolution of the growing front for the first two stages of growth. (e) Typical structure of an MF aggregate.

characterized by $D \to 1$ as $\lambda \to \infty$. This is due to the fact that the radial size of the cluster is small compared to λ. In consequence, the individual interaction regions of the aggregated particles are highly overlapped, forming an almost circular envelope or effective boundary of aggregation around the cluster. This makes the last aggregated particle the most probable aggregation point in the cluster for the next incoming particle. Because of this, there is a tendency for the clusters to develop three main arms or branches, clearly seen as $\lambda \to \infty$. This structural feature is reminiscent of a mean-field (MF) behavior. In the second stage, clusters exhibit a transition in growth dynamics. Here, the envelope starts to develop small deviations from its initial circular form, with typically three main elongations or growth instabilities associated with the main branches. When the distance between the tips of the two adjacent branches becomes of the order of λ, a bifurcation process begins, generating multiscaling growth. Then, when the interactive envelope develops a branched structure itself, particles are able to penetrate into the inner regions of the aggregate and another transition in growth dynamics takes place, from *interaction-limited* to *trajectory-limited*. In the third stage, when the distance among the tips of the main branches becomes much larger than λ, growth is limited by the mean squared displacement of the wandering particles. In this case, the asymptotic value $D = D_0$ and the main features in the global structure of the cluster are remarkably recovered as $N \to \infty$, inheriting the main characteristics of the entropic aggregation-model used, either DLA or BA. That is, even though interactions leave a strong imprint in the local structure and fractality of the clusters, the stochastic nature of the particle trajectories will ultimately determine their global characteristics.

However, taking into account that the spatial size of the clusters is proportional to the radius of gyration $R_g \propto N^{1/D}$, the desired balance between entropic and energetic forces, the latter related to the long-range attractive interaction and to the parameter λ, can be achieved by scaling the interaction range itself with the number of particles in the cluster through $\lambda(N) = \lambda_0 N^{\varepsilon}$, where λ_0 is fixed to one, while ε is the scaling parameter that takes values in [0, 1]; we will refer ε as the *branching* parameter. Given a fixed value of ε and this choice for $\lambda(N)$, every aggregate grown under these conditions has a precise and uniquely defined fractal dimension $D = D(\varepsilon)$. In fact, using $D(\varepsilon)$ for different values of ε, one can define the entropic and energetic ratios given by $f_S = (D(\varepsilon) - 1)/(D_0 - 1)$ and $f_E = 1 - f_S$, respectively, that quantify the specific entropic and energetic contribution to the fractal dimension of the clusters (see **Figure 5**). Here, one can clearly appreciate the transition in growth regimes from entropic, when $\varepsilon \to 0$, to energetic, as $\varepsilon \to 1$, and the nontrivial interplay between them to generate each cluster with a specific dimensionality.

Additionally, this model allows one to estimate $\varepsilon(D)$, in order to grow aggregates with any prescribed fractal dimension D in $[1, D_0]$, once the underlying entropic model, DLA or BA, is selected. As such, we are no longer restricted to the purely entropic models of fractal growth with a constant λ, as the energetic contribution of the long-range attractive interactions is maintained through the varying $\lambda(N)$, enabling one to explore in a continuous manner the full range of clusters with fractal dimensions in $[1, D_0]$. Nonetheless, the purely entropic contribution of the underlying models (DLA or BA) has two important contributions to the clusters' structure: first, they establish an upper limit to the fractal dimensionality (D_0), and second, they define a characteristic morphology to the clusters (that of DLA or BA). This kind of control over the

http://dx.doi.org/10.5772/67941

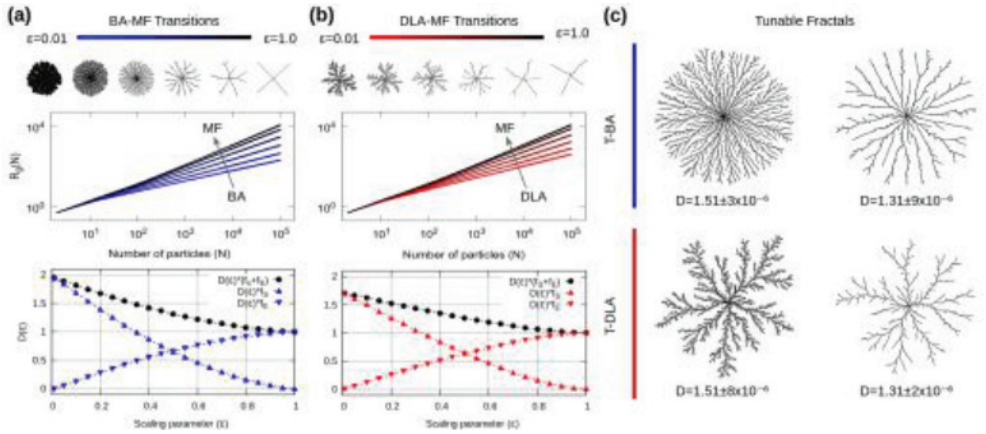

Figure 5. In (a) and (b), aggregates grown with specific values of ε in the interval $[0.01, 1]$ with the λ-model (top row) and log-log plots for R_g (middle row) for (a) BA and (b) DLA with $N = 10^5$ particles. One can appreciate the difference in the morphology of these monofractal-aggregates with respect to ε. Additionally, the specific entropic and energetic contributions to the clusters fractal dimension $D(\varepsilon)$ are shown in the bottom panes. (c) Clusters based in BA (left) and DLA (right) with the same fractal dimension, from top to bottom $D = 1.51$ and 1.31, grown with a very high precision around the desired value.

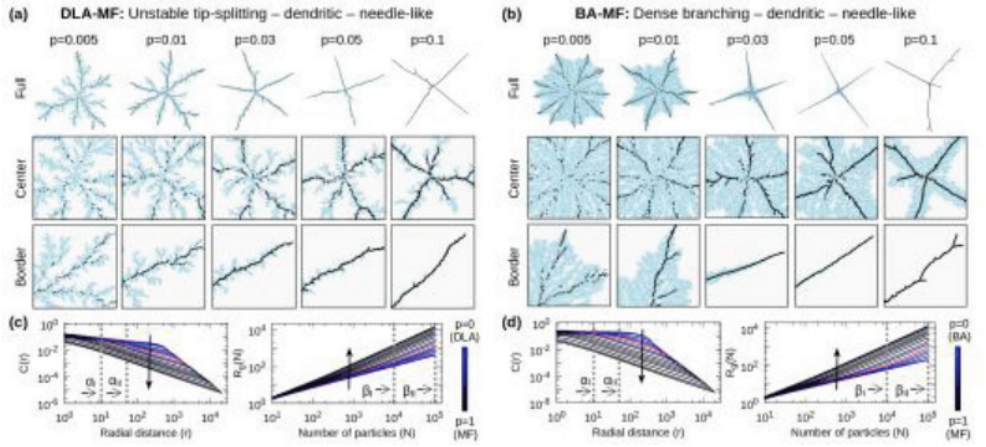

Figure 6. Clusters of 1.5×10^5 particles grown with the indicated values of p, are shown at different magnifications for the (a) DLA-MF and (b) BA-MF transitions. Particles aggregated under DLA/BA are colored in light-grey while those through MF in black. These transitions exhibit fast morphological transformations as p increases, from unstable tip-splitting (DLA) or dense branching (BA), through (inhomogeneous) dendritic, to needle-like growth (MF). (c-d) $C(r)$ and $R_g(N)$ display deviations from a well-defined linear behavior for different p, revealing the inhomogeneity or crossover effects in these clusters. Arrows indicate the direction of the transition as function of p:0→1. This is better seen at low scales, where the stochasticity of DLA or BA dominate the local growth, whereas MF tends to dominate the global morphology as $p \to 1$. In both cases, the dynamical growth-regime changes at $p \approx 0.1$. Labels α_I, α_{II}, β_I, and β_{II} indicate the scales used for the scaling analysis.

clusters' fractal dimension and the range it spans, as well as over the morphology of the clusters, has not been obtained before under any other related scheme of fractality tuning [11].

5.2. The *p*-model: anisotropy-driven transition

In the second approach, a general stochastic aggregation process can be model under a Monte Carlo scheme involving three fundamental and simple *off-lattice* models of particle-cluster aggregation. On one hand, the well-known BA and DLA models provide disordered/fractal structures through their stochastic (entropic) dynamics (**Figure 1a** and **1b**). On the other, we introduce a mean-field (MF) model of long-range interactive particle-cluster aggregation [11, 12] that provides the most energetic (and noiseless) aggregation dynamics that, simultaneously, acts as the main source of anisotropy. We must remark that this anisotropy is purely generated by the growth dynamics and not from lattice effects [28] (see **Figure 1c**). Then, the statistical combination of these models results in an off-lattice DLA-MF and BA-MF dynamics, whose morphological transitions can be controlled by the *mixing* parameter $p \in [0, 1]$, associated with the probability or fraction of particles aggregated under MF dynamics, $p = N_{\mathrm{MF}}/N$, where N is total number of particles in the cluster. Therefore, as p varies from $p = 0$ to $p = 1$, it generates two nontrivial transitions from fractals (DLA) or fat fractals (BA) with fractal dimension $D = D_0$, to nonfractal clusters with $D = 1$ (MF), that capture all the main morphologies of fractal growth [6] (see **Figure 6**).

6. Universal description

It is necessary to remark that the DLA-MF and BA-MF transitions in the p-model are characterized by inhomogeneous clusters, i.e., structures with nonconstant scaling as shown in **Figure 6c** and **d**, in contrast with the ones present in BA-DLA [15, 21] and the DBM [23, 25] characterized by monofractals. These multiscaling features reveal a crossover behavior that can be properly quantified by measuring a local or effective, $D(p)$, at different scales [7], as shown in **Figure 7a** (details for the values of the parameter used to produce **Figure 7** are presented in **Table 1**). Analytically, all measurements can be described by Eqs. (8) and (9), using Λ and χ as fitting parameters. Indeed, the data for $D(p)$ as obtained through to $C(r)$ are very well described by Eq. (8), whereas Eq. (9) better describes the results obtained through $R_g(N)$. In the case of the λ-model, the BA/DLA-MF transitions are governed by the branching parameter, ε, that is equivalent to the mixing parameter p of the p-model. Nonetheless, in the λ-model, the clusters exhibit a monofractal behavior all along the transition as measured by $R_{\mathrm{g}}(N)$. Thus, the data obtained are then described by Eq. (8) as a fitting function. This analysis is presented in **Figure 7d**.

By observing the description of the transitions based on the function $D(q)$ in **Figure 7**, one can clearly appreciate their continuous nature for both the λ- and p-models, as well as the fact that $q = 1$ defines a change in aggregation dynamics from purely entropy to highly energetic. In particular, the similarity between the transitions of BA-MF and those of the DBM is quite interesting, with results such as $D(q) \approx 1$ for $q = 4$ and $D(q) \approx 1.71$ for $q = 1$ in the BA-MF transitions, while $D(\eta) \approx 1$ for $\eta = 4$ and $D(\eta) \approx 1.71$ for $\eta = 1$ in the case of the DBM, even though the processes are different (see **Table 2**). Even more, by plotting all data as a function of $\Phi(q)$ itself, i.e., $D(\Phi)$, the DLA-MF, BA-MF,

http://dx.doi.org/10.5772/67941

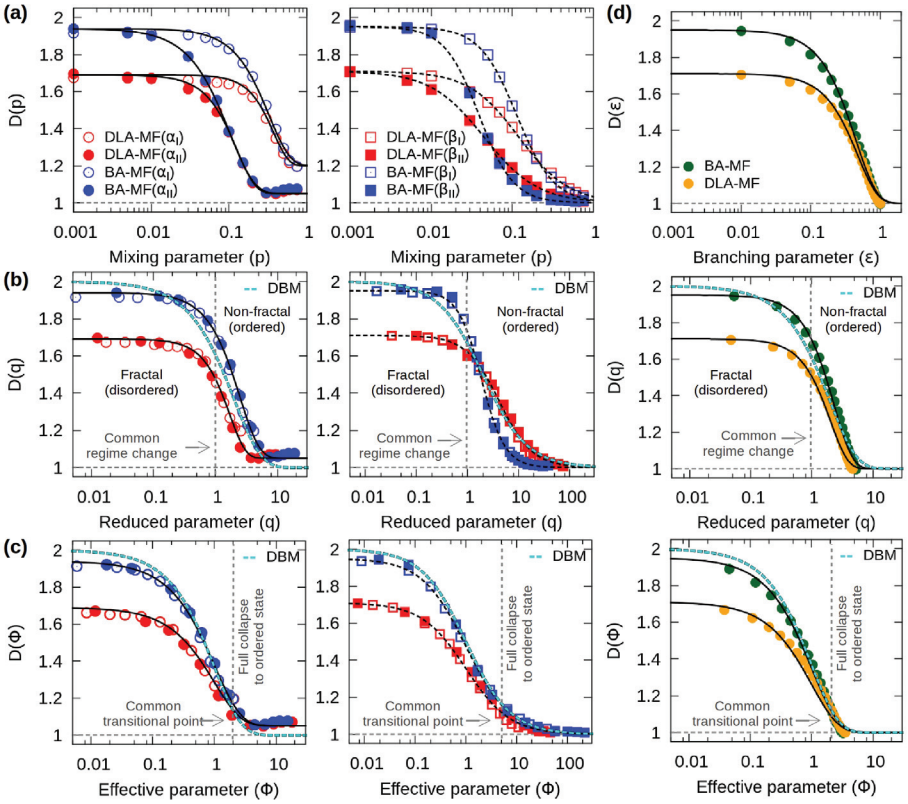

Figure 7. Scaling analysis for the p-model: (a) Plots of $D(p)$ for the DLA-MF and BA-MF transitions obtained from $C(r)$ (left), at small (α_I) and large (α_{II}) scales, and $R_g(N)$ (right), at medium (β_I) and large (β_{II}) scales, in correspondence to **Figures 6c** and **6d**, respectively. These results are described by the solid and dotted curves given by equations (8) and (9), respectively, for different values of the parameters Λ and χ. (b) By plotting D as a function of $q = p/p_i$ (where p_i is calculated for each curve), data collapses into single master curves, $D(q)$, according to Eqs. (10) and (12), respectively. Note the common point of regime change at $q_i = 1$, marked with the vertical dashed lines. The curves for the DBM given by Eqs. (6) and (7), respectively, with $\Lambda = 1$ and $d = d_w = 2$, are also included. (c) In the description with the function $D(\Phi)$, all of the morphological transitions approach common transitional points where clusters have fully collapsed to an ordered structure, independently of the stochastic model used. (d) The corresponding scaling analysis is performed for the BA- and DLA-MF transitions obtained by using the λ-model. In this case, Eqs. (8), (10) and the exponential form of (14), were used. For further details about the parameter values used, see **Table 1**.

and DBM transitions approach the highly anisotropic regime in an almost identical manner, departing from Eqs. (10) and (12). See, for example, **Figure 7c** and the bottom pane in **Figure 7d**.

A final important implication of the previous findings is that the DBM and BA-MF transitions (for both λ- and p-models), even though completely different in origin, could be treated as belonging to the same universality class. To understand this, we must recall that the DBM ($\eta = 1$) and viscous fingering phenomena are said to belong to the same universality class as DLA, because they are all characterized by $D = 1.71$ [10, 29]. Therefore, by extending this idea to the description

with the function $D(\Phi)$ of Eq. (10), the *universality* of these morphological transitions must be understood in the sense that they are described by the same scaling in their fractal dimension. In fact, by defining the reduced codimension, $D^* \in [0,1]$ as $D^* = (D-1)/(D_0-1)$, it is still possible

Model	Transition	Method	Scale	Λ	χ	D_0	p_i, q_i
p	DLA-MF	$C(r)$	α_I	15.4	2.24	1.67	0.29
			α_{II}	71.5	1.82		0.08
		$R_g(N)$	β_I	33.8	1.41	1.71	0.03
			β_{II}	101.6	1.32		0.01
	BA-MF	$C(r)$	α_I	11.6	1.61	1.94	0.18
			α_{II}	45.4	1.38		0.04
		$R_g(N)$	β_I	124.8	1.95	1.95	0.06
			β_{II}	1547.7	2.05		0.02
λ	DLA-MF	$R_g(N)$	10^3 to 10^5	6.10	1.52	1.70	0.21
	BA-MF	$R_g(N)$	10^3 to 10^5	6.35	1.43	1.95	0.19
p	DLA-MF	$C(r)$	–	–	1.69	1.67	1.0
		$R_g(N)$	–	–	1.34	1.71	1.0
	BA-MF	$C(r)$	–	–	1.39	1.94	1.0
		$R_g(N)$	–	–	1.88	1.95	1.0
λ	DLA-MF	$R_g(N)$	–	–	1.52	1.70	1.0
	BA-MF	$R_g(N)$	–	–	1.43	1.95	1.0

In the first block, we present the parameter values used to describe $D(p,\Lambda,\chi)$, using Eqs. (8) and (9). In the second block for Eqs. (10) and (12), used as fitting functions to the $D(q,\chi)$ data obtained through $C(r)$ and $R_g(N)$. In this prescription, χ is the only free parameter to be determined and, by construction, all the inflection points are located at $q = 1$. All of the fittings to the numerical data were performed using the *gnuplot* embedded algorithms.

Table 1. Parameters for the plots of $D(p)$ and $D(q)$ in **Figure 7**.

Model	Data	D_0	χ	$\Phi_t(v = 0.1)$	q_t	$\Phi_t(v = 0.05)$	q_t	$D(q = 1)$
p	BA-MF (α)	1.94	1.39	2.3	4.5	3.0	5.4	1.72
	DLA-MF (α)	1.67	1.69	2.3	2.8	3.0	3.2	1.46
	BA-MF (β)	1.95	1.88	9.0	6.0	19.0	9.0	1.73
	DLA-MF (β)	1.71	1.34	9.0	21.7	19.0	37.8	1.62
λ	BA-MF	1.95	1.43	2.3	4.2	3.0	5.0	1.70
	DLA-MF	1.71	1.52	2.3	3.5	3.0	4.2	1.50

The labels α and β indicate that these data were obtained through measurements of the fractal dimension using $C(r)$ and $R_g(N)$, respectively.

Table 2. Transitional points for which the reduced co-dimension $D^* \approx 0$ for the λ- and p-models studied in this work.

http://dx.doi.org/10.5772/67941

to define the ultimate representation for the scaling of the transitions through the reduced codimensionality functions. From Eqs. (10) and (12), these are, respectively given by,

$$D^*(\Phi) = e^{-\Phi}, \tag{14}$$

$$D^*(\Phi)^{(1)} = \frac{1}{1+\Phi}, \tag{15}$$

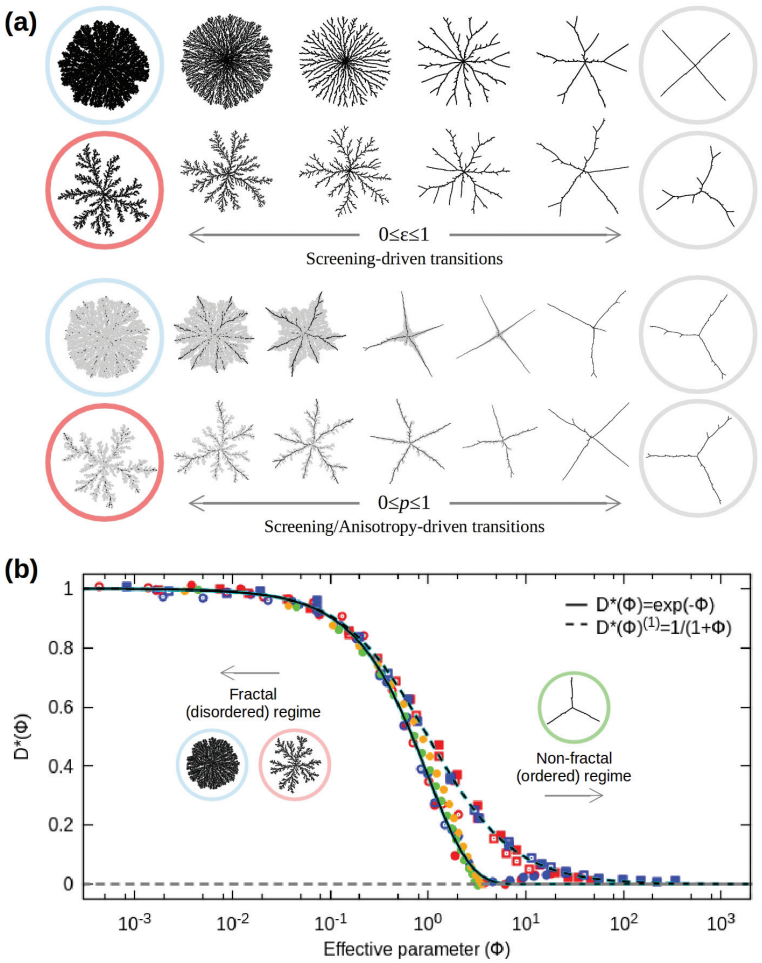

Figure 8. (a) Snapshots of typical clusters present in fractal to nonfractal morphological transitions obtained from the λ-model with the branching parameter ε as the control parameter, and the p-model with the mixing parameter p as the control parameter. (b) By plotting $D^*(\Phi)$ and $D^*(\Phi)^{(1)}$, the data for the morphological transitions DLA-MF, BA-MF, and DBM collapse to universal curves described by Eqs. (14) and (15). Under this prescription, these universal fractal to nonfractal morphological transitions are independent of the initial fractal dimension, D_0, the symmetry-breaking process that drives the transition, even crossover effects, and, quite remarkably, the Euclidean dimension, d, of its embedding space. All of the numerical data comes from **Figure 7**.

where the effective parameter Φ is, respectively, given by Eqs. (11) and (13) for each of the previous two equations. Notice that, since the morphological transitions presented in this work are independent of their symmetry-breaking processes, initial-configuration, and that D_0 is given by the HTM equation, we arrive to the important conclusion that, under the formalism based on Eqs. (14) and (15), fractal to nonfractal morphological transitions will follow the same curves independently of the Euclidean dimension of the embedding space, as shown in **Figure 8**. This finding makes it clear that it is possible to define *universal* transitional point, Φ_t, where the screening/anisotropy effects are dominant over the morphology of the cluster and $D \approx 1$. Starting with reduced codimension at Φ_t, i.e., $D_t^* = (D(\Phi_t) - 1)/(D_0 - 1) = \nu$, we can ask for the condition $\nu \ll 1$ to be fulfilled (see **Figure 8**). Then, the universal transitional points, Φ_t, must, respectively satisfy $\exp(-\Phi_t) = \nu$ and $\Phi_t = (1 - \nu)/\nu$ for the Eqs. (14) and (15). In order to recover the particular transitional points for Eqs. (10) and (12), we must recall that $\Phi_t = \Phi(q_t)$ and thus, one has to solve for q_t. Notice also that $q_t = q_t(\nu, \chi, D_0)$, therefore it gives different values for each transition (see **Table 2**).

7. Conclusion

It has been stated above that the entropic and energetic elements are the two aspects of the complex aggregation dynamics which in nature are strongly correlated. Nonetheless, this reductionist approach that essentially encapsulates the information of all the finer details of the dynamics into an effective interaction (in the λ-model, for example) or through a Monte Carlo approach to aggregation (as in the p-model) has proven to be quite rewarding, as one can appreciate the wide assortment of fractal morphologies that can be generated and the fine and easy control one can achieve by means of a single parameter. Here, we shall recall that in two-dimensional systems ($d = 2$), by changing the fractal dimension of the particle trajectories, d_w, from $d_w = 2$ (random) to 1 (ballistic), it is possible to generate a complete set of clusters with fractal dimension between $D = 1.71$ (DLA) to 2 (BA), corresponding to the stochastic (entropic) regime. However, by scaling the interaction range λ with N, or by gradually introducing an energetic element trough MF dynamics, we are no longer restricted to this range in D as we were. We can now explore the full set of fractals with D in $[1, D_0]$, where D_0 ranges from that value corresponding to DLA to that corresponding to BA, not necessarily bound to $d = 2$, since these approaches can be easily extended to higher dimensions [30].

Additionally, the descriptive framework for the scaling of fractal to nonfractal morphological transitions in stochastic growth processes, which includes the concept of an effective screening/anisotropy force and reduced codimensionality transformations, has revealed that the DLA-MF, BA-MF, and DBM transitions exhibit a well-defined universal scaling $D^*(\Phi)$, which is independent of the initial fractal configuration of the system, the dimensionality of the embedding space, crossover effects, and the anisotropy force acting upon them.

The results and models discussed in this chapter represent an important unifying step toward a complete scaling theory of fractal growth and far-from-equilibrium pattern formation. Additionally, the possibility of applying the dimensionality function to discuss complex structures in other research areas, ranging from biology [4, 1], intelligent materials engineering [31, 32] to medicine [33], seems to be in some cases straightforward.

Acknowledgements

The authors gratefully acknowledge the computing time granted on the supercomputers MIZTLI (DGTIC-UNAM) and THUBAT-KAAL (CNS-IPICyT) and on XIUHCOATL (CINVESTAV) through M.A. Rodriguez (ININ, Mexico). We acknowledge the partial financial support by CONACyT and VIEP-BUAP through the grants: 257352, DIRV-EXC16-I, and CAEJ-EXC16-G.

Author details

José Roberto Nicolás-Carlock[1], Víctor Dossetti[2] and José Luis Carrillo-Estrada[1]*

*Address all correspondence to: carrillo@ifuap.buap.mx

1 Physics Institute, Autonomous University of Puebla, México

2 CIDS-Instituto de Ciencias, Autonomous University of Puebla, Mexico

References

[1] Ben-Jacob E. From snowflake formation to growth of bacterial colonies. Part I. Diffusive patterning in azoic systems. Contemporary Physics. 1993; **34**:247–273. DOI: 10.1080/00107519308222085

[2] Ben-Jacob E. From snowflake formation to growth of bacterial colonies. Part II. Cooperative formation of complex colonial patterns. Contemporary Physics. 1997; **38**:205–241. DOI: 10.1080/001075197182405

[3] Ronellenfitsch H, Katifori E. Global optimization, local adaptation, and the role of growth in distribution networks. Physical Review Letters. 2016; **117**:138301. DOI: 10.1103/PhysRevLett.117.138301

[4] Vicsek T. Fluctuations and scaling in biology. Oxford University Press, New York, 2001.

[5] Ben-Jacob E, Garik P. The formation of patterns in nonequilibrium growth. Nature. 1990; **343**:523–530. DOI: 10.1038/343523a0

[6] Vicsek T. Fractal growth phenomena. World Scientific, Singapore, 1992.

[7] Meakin P. Fractals, scaling and growth far from equilibrium. Cambridge University Press, United Kingdom, 1998.

[8] Sander L M. Fractal growth processes. Nature. 1986; **322**:789–793. DOI: 10.1038/322789a0

[9] Sander L M. Diffusion-limited aggregation: A kinetic critical phenomenon? Contemporary Physics. 2000; **41**:203–218. DOI: 10.1080/001075100409698

[10] Sander L M. Fractal growth processes. In: Meyers R A, editor. Mathematics of complexity and dynamical systems. Springer, New York, 2011. 429 p. DOI: 10.1007/978-0-387-30440-3

[11] Nicolás-Carlock J R, Carrillo-Estrada J L, Dossetti V. Fractality à la carte: a general particle aggregation model. Scientific Reports. 2016; **6**:19505. DOI: 10.1038/srep19505

[12] Nicolás-Carlock J R, Carrillo-Estrada J L, Dossetti V. Universality of fractal to non-fractal morphological transitions in stochastic growth processes. Arxiv. [Preprint] 2016. Available from: https://arxiv.org/abs/1605.08967

[13] Muthukumar M. Mean-field theory for diffusion-limited cluster formation. Physical Review Letters. 1983; **50**:839. DOI: 10.1103/PhysRevLett.50.839

[14] Tokuyama M, Kawasaki K. Fractal dimensions for diffusion-limited aggregation. Physics Letters. 1984; **100A**:337. DOI: 10.1016/0375-9601(84)91083-1

[15] Meakin P. Cluster-particle aggregation with fractal (Levy flight) particle trajectories. Physical Review B. 1984; **29**:3722. DOI: 10.1103/PhysRevB.29.3722

[16] Honda K, Toyoki H, Matsushita M. A Theory of fractal dimensionality for generalized diffusion-limited aggregation. Journal of the Physical Society of Japan. 1986; **55**:707–710. DOI: 10.1143/JPSJ.55.707

[17] Matsushita M, Honda K, Toyoki H, Hayakawa Y, Kondo H. Generalization and the fractal dimensionality of diffusion-limited aggregation. Journal of the Physical Society of Japan. 1986; **55**:2618–2626. DOI: 10.1143/JPSJ.55.2618

[18] Meakin P. Effects of particle drift on diffusion-limited aggregation. Physical Review B. 1983; **28**:5221. DOI: 10.1103/PhysRevB.28.5221

[19] Huang Y-B, Somasundaran P. Effects of random-walk size on the structure of diffusion-limited aggregates. Physical Review A. 1987; **36**:4518–4521. DOI: 10.1103/PhysRevA.36.4518

[20] Huang S-Y, Zou X-W, Tan Z-J, Jin Z-Z. Particle-cluster aggregation by randomness and directive correlation of particle motion. Physics Letters A. 2001; **292**:141–145. DOI: 10.1016/S0375-9601(01)00761-7

[21] Ferreira Jr S C, Alves S G, Faissal B A, Moreira J G. Morphological transition between diffusion-limited and ballistic aggregation growth patterns. Physical Review E. 2005; **71**:051402. DOI: 10.1103/PhysRevE.71.051402

[22] Alves S G, Ferreira Jr S C. Aggregation in a mixture of Brownian and ballistic wandering particles. Physical Review E. 2006; **73**:051401. DOI: 10.1103/PhysRevE.73.051401

[23] Niemeyer L, Pietronero L, Wiesmann H J. Fractal dimension of dielectric breakdown. Physical Review Letters. 1984; **52**:1033. DOI: 10.1103/PhysRevLett.52.1033

[24] Pietronero L, Erzan A, Evertsz C. Theory of fractal growth. Physical Review Letters. 1988; **61**:861. DOI: 10.1103/PhysRevLett.61.861

[25] Sánchez A, et al. Growth and forms of Laplacian aggregates. Physical Review E. 1993; **48**:1296. DOI: 10.1103/PhysRevE.48.1296

[26] Hastings M B. Fractal to non-fractal phase transition in the dielectric breakdown model. Physical Review Letters. 2001; **87**:175502. DOI: 10.1103/PhysRevLett.87.175502

[27] Hayakawa Y, Kondo H, Matsushita M. Monte Carlo simulations of the generalized diffusion-limited aggregation. Journal of the Physical Society of Japan. 1986; **55**:2479–2482. DOI: 10.1143/JPSJ.55.2479

[28] Meakin P. Noise-reduced and anisotropy-enhanced Eden and screened-growth models. Physical Review A. 1988; **38**:418. DOI: 10.1103/PhysRevA.38.418

[29] Mathiesen J, Procaccia I, Swinney H L, Thrasher M. The universality class of diffusion-limited aggregation and viscous fingering. Europhysics Letters. 2006; **72**:257–263. DOI: 10.1209/epl/i2006-10246-x

[30] Tolman S, Meakin P. Off-lattice and hypercubic-lattice models for diffusion-limited aggregation in dimensionalities 2–8. Physical Review A. 1989; **40**:428–437. DOI: 10.1103/PhysRevA.40.428

[31] Lehn J-M. Toward self-organization and complex matter. Science. 2002; **295**:2400. DOI: 10.1126/science.1071063

[32] Whitesides G M, Grzybowski B. Self-assembly at all scales. Science. 2002; **295**:2418. DOI: 10.1126/science.1070821

[33] Sturmberg J P, West B J. Fractals in physiology and medicine. In: Sturmberg J P, Martin C M, editors. Handbook of systems and complexity in health. Springer, New York; 2013. 171 p. DOI: 10.1007/978-1-4614-4998-0